Glacial discharge along the west Antarctic Peninsula during the Holocene

Jennifer Pike[1], George E.A. Swann[2], Melanie J. Leng[3,4] and Andrea M. Snelling[4]

[1]School of Earth and Ocean Sciences, Cardiff University, Main Building, Park Place, Cardiff CF10 3AT, UK. Tel: +44 (0)29 2087 5181; Fax: +44 (0)29 2087 4326; pikej@cardiff.ac.uk
[2]School of Geography, University of Nottingham, University Park, Nottingham, NG7 2RD, UK. Tel: +44 (0)115 846 6768; Fax: +44 (0)115 951 5249; george.swann@nottingham.ac.uk
[3]Department of Geology, University of Leicester, Leicester, LE1 7RH, UK. Tel: +44 (0)115 936 3515; Fax: +44 (0)115 936 3002; mjl@bgs.ac.uk
[4]NERC Isotope Geosciences Laboratory, British Geological Survey, Keyworth, Nottingham, NG12 5GG, UK. Tel: +44 (0)115 936 3426; Fax: +44 (0)115 936 3002; asnel@bgs.ac.uk

In light of recent instrumental records of warming along the Antarctic Peninsula[1], there has been much debate about what has influenced rising temperatures during the late Holocene, with mechanisms ranging from variations in the westerly winds that cause upwelling of warm deep waters onto the continental shelf[2] to the influence of El Niño – Southern Oscillation on sea surface temperatures[3]. Here, we present a Holocene glacial discharge record derived from the oxygen isotope composition of marine diatoms from the west Antarctic Peninsula continental margin. Our results provide a unique opportunity to assess atmospheric versus oceanic influence on glacial discharge because analysis of diatom geochemistry provides information about atmospherically-forced glacial ice discharge whilst diatom assemblage[4] ecology provides information about the oceanic environment. We show that increasing occurrence of La Niña[5] and increasing summer insolation, atmospheric forcing, had a stronger influence on glacial discharge to the west Antarctic Peninsula margin during the late Holocene than oceanic processes driven by southern westerly winds and upwelling of upper circumpolar deepwater. Given uncertainty about the future evolution of El Niño – Southern Oscillation under global warming[6], it remains to be established how these changes will impact on the climatically-sensitive system of the Antarctic Peninsula Ice Sheet.

World-wide, the west Antarctic Peninsula (WAP) has experienced one of the greatest and fastest rates of atmospheric warming since observations began[1]. Much of the increase in surface air temperature has been attributed to an atmospheric circulation pattern characterised by a positive Southern Annular Mode (SAM)[1]. However, the warming trend began prior to the recent positive phase of the SAM[1], so other factors must also be contributing to WAP warming. Concomitant with the processes that are proposed for atmospheric warming (and involved in a positive feedback loop

with those processes), mean surface ocean temperatures have increased by >1°C[7]. All of these factors have contributed to the retreat of 87% of marine glacier fronts along the WAP over the past six decades[8]. Given likely future increased melting rates due to anthropogenic warming, we place these contemporary observations into their historical context by analysing the oxygen isotope composition of marine diatom silica ($\delta^{18}O_{diatom}$) from 13.0-0.3 ka (Fig. 1a). We show that from 3.6-0.3 ka, glacial ice discharge (icebergs/brash ice) to the WAP increased and was most likely related to the increasing strength of the El Niño – Southern Oscillation (ENSO) circulation pattern of the Pacific Ocean and peak summer insolation.

We interpret our $\delta^{18}O_{diatom}$ record (Fig. 1a) from Palmer Deep, WAP (ODP Site 1098A, 64°51.72'S, 64°12.47'W)[9] as being forced by variations in glacial discharge ($\delta^{18}O < –20‰$) and our record, together with planktonic diatom assemblage data[4], provides a unique opportunity to assess the relative contributions to past glacial discharge of (i) glacial ice discharge forced by atmospheric processes, and (ii) frontal melt (of floating glaciers/ice shelves) driven by oceanic warmth. Over our record, the base shows the most intense period of deglaciation in the Palmer Deep region (13.0-12.1 ka; lowest bulk $\delta^{18}O_{diatom}$ +38.3‰, mean = +41.3±1.8‰ [± 1 s.d.], Fig. 1a). This peak glacial discharge to the coastal margin was co-incident with ice sheet retreat across the outer[10] and inner[11] Anvers Shelf, the break-up of the Marguerite Bay ice shelf to the south[12] and the transition from perennial to seasonal sea ice in Maxwell Bay to the north[13] (Fig. S1). Increased upwelling of upper Circumpolar Deepwater (UCDW) onto the continental shelf at this time[14] associated with strong winds in the southern region of the Southern Hemisphere westerlies[15] (Fig. 1g) would have supplied additional warmth to the upper water column making frontal melting the dominant mechanism driving glacial discharge/$\delta^{18}O_{diatom}$.

Between 12.1-11.5 ka, higher $\delta^{18}O_{diatom}$ (mean = +42.8±0.2‰) suggests a slow-down in glacial discharge to the WAP shelf (Fig 1a). Following this reversal, $\delta^{18}O_{diatom}$ declined between 11.5-9.0 ka (mean = +41.8±0.8‰) indicating prolonged and increasing influx of glacial discharge (Fig. 1a) during a time of widespread warmth along the WAP exemplified by ice sheet retreat and thinning[2], high SSTs[3] and thin sea ice cover with warm winters[4] in Palmer Deep, the collapse of the George VI Ice Shelf (Fig. S1) at 9.6 ka[16] and increased influence of glacial melt and precipitation in Maxwell Bay[13]. This warmth was concomitant with the last influence of orbitally-forced deglaciation[5,15] and ENSO-sensitive proxy records from the Peru margin and Ecuador[5,17] that indicate a persistent warm, mean La Niña-like state (relative to mean El Niño-like conditions). Hence, an atmospheric link between ENSO-like tropical Pacific climate variability and the WAP may have been delivering atmospheric warmth and driving glacial ice discharge to the WAP at this time, as well as UCDW upwelling driving frontal melting (Figs. 2a,d, and e). $\delta^{18}O_{diatom}$ (Fig. 1a) steadily increased between ~9.0-6.7 ka (mean = +42.0±0.6‰), indicating a slowdown in glacial

discharge following early Holocene warmth, and was relatively stable between 6.7-5.0 ka (mean = +42.4±0.6‰) (Fig. 1a), with occasional moderate excursions suggesting abrupt increases in iceberg calving. From 9.0-5.0 ka reductions in diatoms that prefer cool, ice-rich surface waters through summer, increases in diatoms associated with spring sea ice melt water stratification[4] and the persistent presence of UCDW at Palmer Deep[18] suggests that ocean-driven frontal melting of floating glaciers and ice shelves made a significant contribution to glacial discharge.

From 5.0-3.6 ka, there was a notable shift to increased variability in $\delta^{18}O_{diatom}$ (mean = +42.1±0.8‰) that reflects the increased occurrence of large (c. 2‰) multicentennial fluctuations in glacial discharge to the WAP (Fig. 1a). Following the onset of this variability, Antarctic Peninsula terrestrial records also show significant warmth between 4.5-2.8 ka[2 and references therein] which suggests an increasing, but variable, influence of glacial ice, hence atmospheric forcing, on glacial discharge to the WAP. Morlet wavelet analysis (Supplementary Information) of our $\delta^{18}O_{diatom}$ data shows a significant increase in the power of these multicentennial fluctuations with a period of 400-500 yr after 5.0 ka (Fig. 2). Increased variability and periodicity are also observed from c. 5.0 ka in many other Southern Hemisphere palaeoclimate records and are linked to movement of the inter-tropical convergence zone (ITCZ)[19] combined with increasing ENSO activity[17,20] (Fig. 1c), the position and strength of the Southern Hemisphere westerlies[15] (Fig. 1g), upwelling of UCDW onto the WAP shelf and cyclonic activity[21], and rapid shifts between warm and cold sea surface conditions along the WAP[4] (Fig. 1b). This increased $\delta^{18}O_{diatom}$ variability also coincided with a mid-Holocene transition in the regulation of Antarctic climate from being dominated by non-cyclic forcing to cyclic internal forcing[14]. An abrupt increase in Peru margin climate variability, at multicentennial-scale and recorded in ENSO-sensitive proxies, took place between 5.4-4.6 ka[19] and was ascribed to a combination of the ITCZ moving southwards away from the equator and changes in the source region of the tropical thermocline waters, i.e. Antarctic Intermediate Water, sourced from around the Antarctic margin[19]. The multicentennial period variability in our Antarctic $\delta^{18}O_{diatom}$ record (Fig. 2) supports this interpretation and provides additional evidence for an eastern Pacific Ocean-Southern Ocean centennial-scale ocean teleconnection following the mid-Holocene transition.

From 3.6-0.3 ka, $\delta^{18}O_{diatom}$ continued to record multicentennial fluctuations in glacial discharge, and also shows an underlying decrease towards lower values, particularly from c. 2.5 ka (Fig. 1a; 3.6-0.3 ka: $\delta^{18}O_{diatom}$ mean = +41.7±0.8‰). We interpret this decrease as increasing glacial ice discharge rather than frontal melting because the persistent presence of warm UCDW in Palmer Deep ended at c. 3.6 ka[18] and diatom concentration and assemblage data indicate cooler SSTs and less spring sea ice melt-induced stratification after this time[4,22]. Increased glacial ice discharge was driven by atmospheric warming of the WAP and increased moisture delivery as a result of two forcing mechanisms; maximum Holocene ENSO frequency from c. 2.2 ka[5,17,20] (Fig.

1c-e) and increased La Niña intensity[23] (Fig. 1d), coupled with peak summer insolation at 60ºS[24] (Fig. 1f). Our $\delta^{18}O_{diatom}$ interpretation of atmospheric warmth driving glacial ice discharge over the last 3.6 ka is consistent with diatom assemblages that show low concentrations, low productivity and, in general, icier sea surface conditions[4] because delivery of oceanic warmth by UCDW upwelling was variable and increased glacial ice discharge to the coastal ocean further acted to cool surface waters. From 2.5 ka biological indicators show decreased lacustrine productivity (interpreted as cooling[2 for a summary]) but are likely to be responding to decreasing spring insolation and so do not contradict our $\delta^{18}O_{diatom}$ interpretation. Our increase in glacial discharge is cyclic and includes cooler periods that may be related to regionally-variable glacier advances during this period[18]. Our unique combination of atmospheric ($\delta^{18}O_{diatom}$) and oceanic (diatom assemblages[4]) proxies provides the first direct evidence to support the suggestion that the terrestrial and marine environments of the WAP are responding to different primary forcings[2] and enables examination of the relative influence of glacial ice discharge versus frontal melt in the past. The oceanic proxies respond strongly to spring insolation (peak 8.0-6.0 ka[24]) and the delivery of warmth from upwelling UCDW (that would influence the frontal melt component of glacial discharge), whereas the terrestrial environment and glacial ice discharge is strongly linked with changes in tropical Pacific SSTs via atmospheric teleconnections[25] and with summer insolation (peak c. 2.0 ka[24]) (Supplementary Information and Fig. S4). The pattern of ENSO circulation is teleconnected to Antarctic climate, in particular the Amundsen Sea Low (ASL) pressure region, via movements of the South Pacific Convergence Zone (SPCZ)[26], an atmospheric Rossby wave train and the Antarctic Dipole[25]. La Niña events are accompanied by a northerly shift in the SPCZ and the production of cyclones in the region of the ASL, which produce a warm, northerly air flow over the WAP[1]. Weaker winds in the southern region of the Southern Hemisphere westerlies after c. 3.5 ka[15] (Fig. 1g), following the shift of the westerly wind belt northwards at c. 5.0 ka (Debret et al. 2009), would normally have promoted dry, cooler conditions along the WAP, however, our record shows an increase in glacial ice discharge, particularly after c. 2.5 ka (Fig. 1a). This increase reflects continued atmospheric warming when the ENSO pattern was strong and La Niña was enhanced, especially relative to El Niño during the period between 2.0-1.0 ka[5]. A late Holocene link between La Niña and WAP SST via oceanic forcing has been suggested beginning 1.7 ka[3], however, this is based on comparisons with a proxy ENSO record that is insensitive to variations in the strength of La Niña[20] and the reconstructed high SSTs from 1.7 ka are inconsistent with diatom assemblage and concentration data that show evidence for extensive sea ice, cooler SSTs and reduced spring sea ice-melt water stratification at this time[4] (Fig. S3). The resemblance of multicentennial periodicity between $\delta^{18}O_{diatom}$ (Fig. 2) and a Pacific ENSO record[17] provides strong evidence that a direct atmospheric teleconnection between the low latitude Pacific and Antarctic Peninsula Ice Sheet

(APIS) discharge existed since at least 2.5 ka. This strengthens our proposition that La Niña, together with summer insolation, exerted a strong atmospheric forcing on ice sheet dynamics and glacial discharge along the WAP from 3.6-0.3 ka that was more important than mechanisms involving changes in the southern westerlies and ocean circulation.

Although the warming along the WAP over the past century cannot solely be attributed to the SAM, the teleconnection between ENSO and the WAP atmospheric circulation is strongest when it is in phase with the SAM[1]. Here we extend this observation into the geological record and show that increased ENSO variability from 3.6-0.3 ka, particularly enhanced La Niña activity, augmented the opportunity for constructive interference of the SAM and ENSO during a period of peak summer insolation, all of which together are responsible for the underlying increase in glacial discharge seen in our record. Given recent research investigating the potential future evolution of the ENSO system under global warming[6], it seems likely that changes in ENSO will continue to impact on the Antarctic ice sheets which, in recent decades[25], have also come under the increasing influence of the southern westerly winds with greater volumes of UCDW on the continental shelf accelerating frontal melting of glaciers and basal melting of ice shelves[8,25,27].

Methods

To construct our $\delta^{18}O_{diatom}$ record, diatoms were extracted from the sediments, purified and analysed for $\delta^{18}O_{diatom}$ using a step-wise fluorination procedure (replicate analysis of sample material indicates an analytical reproducibility of 0.3‰ (1σ); see Supplementary Information for further detail). We interpret our $\delta^{18}O_{diatom}$ record as being forced by variations in meteoric water flux[28] with glacial discharge (iceberg/brash ice melt and floating glacier/ice shelf basal melting) being volumetrically more important than inputs (i.e. from the surface snow layer) introduced by the seasonal melting of sea ice[28]. Further, from modern observations on the WAP, the dominant seasonal shift in surface water $\delta^{18}O$ occurs with the summer glacial discharge to the coastal ocean and not the spring sea ice-derived snow melt[28], hence, we are confident that glacial discharge is the dominant driver of our $\delta^{18}O_{diatom}$ record. Modern ice-free seasonal sea surface temperature (SST) variations along the WAP shelf of 2°C only account for up to 0.4‰ of the $\delta^{18}O_{diatom}$ variability and, correcting for Holocene changes[3], we show that SST has little impact on $\delta^{18}O_{diatom}$ (Supplementary Fig. S3). Hence, we can use $\delta^{18}O_{diatom}$ to monitor Holocene glacial discharge along the WAP (Fig. 1a). Extremely high post-glacial (13.0-12.0 ka) sedimentation rates in Palmer Deep (2.32 cm yr^{-1}) and the preservation of annually laminated sediments[29] allows single taxon $\delta^{18}O_{diatom}$ samples to be concentrated from individual laminations of near-single-taxa composition and analysed to provide an insight into the seasonality of glacial discharge and melt water input to the margin at that time[30]. These analyses on individual laminations reveal that the variability in bulk species $\delta^{18}O_{diatom}$ samples over the last deglaciation (5.0‰, Fig. 1a) can be accounted for by glacial discharge during summer and lower contributions in spring[30], which follows the pattern of modern observations[28].

References

1 Russell, A. & McGregor, G. R. Southern hemisphere atmospheric circulation: impacts on Antarctic climate and reconstructions from Antarctic ice core data. *Clim. Change* **99**, 155-192 (2010).

2 Bentley, M. J. *et al.* Mechanisms of Holocene palaeoenvironmental change in the Antarctic Peninsula region. *The Holocene* **19**, 51-69 (2009).

3 Shevenell, A. E., Ingalls, A. E., Domack, E. W. & Kelly, C. Holocene Southern Ocean surface temperature variability west of the Antarctic Peninsula. *Nature* **470**, 250-254 (2011).

4 Taylor, F. & Sjunneskog, C. Postglacial marine diatom record of the Palmer Deep, Antarctic Peninsula (ODP Leg 178, Site 1089), 2, diatom assemblages. *Paleoceanogr.* **17**, DOI 10.1029/2000PA000564 (2002).

5 Makou, M. C., Eglinton, T. I., Oppo, D. W. & Hughen, K. A. Postglacial changes in El Niño and La Niña behavior. *Geology* **38**, 43-46 (2010).

6 Yeh, S.-W. *et al.* El Niño in a changing climate. *Nature* **461**, 511-514 (2009).

7 Meredith, M. P. & King, J. C. Rapid climate change in the ocean west of the Antarctic Peninsula during the second half of the 20th century. *Geophys. Res. Lett.* **32**, L19604, doi:19610.11029/12005GL024042 (2005).

8 Cook, A. J., Fox, A. J., Vaughan, D. G. & Ferrigno, J. G. Retreating glacier fronts on the Antarctic Penisula over the past half-century. *Science* **308**, 541-544 (2005).

9 Barker, P. F., Camerlenghi, A., Acton, G. D. et al. *Proceedings of ODP, Initial Reports, 178 (CD-ROM)*. (Available from: Ocean Drilling Program, Texas A&M University, College Station, TX 77845-9547, 1999).
10 Heroy, D. C. & Anderson, J. B. Radiocarbon constraints on Antarctic Peninsula Ice Sheet retreat following the Last Glacial Maximum (LGM). *Quat. Sci. Rev.* **26**, 3286-3297 (2007).
11 Domack, E. *et al.* Chronology of the Palmer Deep site, Antarctic Peninsula: A Holocene paleoenvironmental reference for the circum-Antarctic. *The Holocene* **11**, 1-9 (2001).
12 Kilfeather, A. A. *et al.* Ice-stream retreat and ice-shelf history in Marguerite Trough, Antarctic Penisula: Sedimentological and foraminiferal signatures. *Geol. Soc. Am. Bull.* **123**, 997-1015 (2011).
13 Milliken, K. T., Anderson, J. B., Wellner, J. S., Bohaty, S. M. & Manley, P. L. High-resolution Holocene climate record from Maxwell Bay, South Shetland Islands, Antarctica. *Geol. Soc. Am. Bull.* **121**, 1711-1725 (2009).
14 Debret, M. *et al.* Evidence from wavelet analysis for a mid-Holocene transition in global climate forcing. *Quat. Sci. Rev.* **28**, 2675-2688 (2009).
15 Lamy, F. *et al.* Holocene changes in the position and intensity of the southern westerly wind belt. *Nature Geosci.* **3**, 695-699 (2010).
16 Roberts, S. J. *et al.* The Holocene history of George VI Ice Shelf, Antarctic Peninsula from clast-provenance analysis of epishelf sediments. *Palaeogeogr. Palaeoclimatol. Palaeoecol.* **259**, 258-283 (2008).
17 Moy, C. M., Seltzer, G. O. & Rodbell, D. T. Variability of El Niño/Southern Oscillation activity at millennial timescales during the Holocene epoch. *Nature* **420**, 162-165 (2002).
18 Domack, E. W. in *Proceedings of the Ocean Drilling Program, Leg 178, Scientific Results* (eds P. F. Barker, A. Camerlenghi, G. D. Acton, & A. T. S. Ramsay) (Ocean Drilling Program, Texas A&M University, 2002).
19 Chazen, C. R., Altabet, M. A. & Herbert, T. D. Abrupt mid-Holocene onset of centennial-scale climate variability on the Peru-Chile Margin. *Geophys. Res. Lett.* **36**, L18704, doi:18710.11029/12009GL039749 (2009).
20 Conroy, J. L., Overpeck, J. T., Cole, J. E., Shanahan, T. M. & Steinitz-Kannan, M. Holocene changes in eastern tropical Pacific climate inferred from a Galápagos lake sediment record. *Quat. Sci. Rev.* **27**, 1166-1180 (2008).
21 Willmott, V. *et al.* Holocene changes in *Proboscia* diatom productivity in shelf waters of the north-western Antarctic Peninsula *Ant. Sci.* **22**, 3-10 (2010).
22 Leventer, A. *et al.* Productivity cycles of 200-300 years in the Antarctic Peninsula region: Understanding linkages among the sun, atmosphere, oceans, sea ice, and biota. *Geol. Soc. Am. Bull.* **108**, 1626-1644 (1996).
23 Khider, D., Stott, L. D., Emile-Geay, J., Thunell, R. & Hammond, D. E. Assessing El Niño Southern Oscillation variability during the last millennium. *Paleoceanogr.* **26**, PA3222, doi:3210.1029/2011PA002139 (2011).
24 Berger, A. & Loutre, M. F. Insolation values for the climate of the last 10 million years. *Quat. Sci. Rev.* **10**, 297-317 (1991).
25 Ding, Q., Steig, E. J., Battisti, D. J. & Küttel, M. Winter warming in West Antarctica caused by central tropical Pacific warming. *Nature Geosci.* **4**, 398-403 (2011).
26 Renwick, J. A. Persistent positive anomalies in the Southern Hemisphere circulation. *Mon. Weather Rev.* **133**, 977-988 (2005).
27 Pritchard, H. D. *et al.* Antarctic ice-sheet loss driven by basal melting of ice shelves. *Nature* **484**, 502-505 (2012).
28 Meredith, M. P. *et al.* Changes in freshwater composition of the upper ocean west of the Antarctic Peninsula during the first decade of the 21st century. *Progress in Oceanography* **87**, 127-143 (2010).
29 Maddison, E. J., Pike, J., Leventer, A. & Domack, E. W. Deglacial seasonal and sub-seasonal diatom record from Palmer Deep, Antarctica. *J. Quat. Sci.* **20**, 435-446 (2005).
30 Swann, G. E. A., Pike, J., Snelling, A. & Leng, M. J. Seasonally-resolved diatom $\delta^{18}O$ records from the west Antarctic Peninsula over the last deglaciation. *Earth Planet. Sci. Lett.* (submitted).

Acknowledgements

We thank H. J. Sloane for assistance with the isotope analyses, I. M. Thomas for assistance with wavelet analysis, staff at the IODP Gulf Coast Core Repository for assistance with sampling ODP Site 1098 and S. Barker, C. Sjunneskog and M. Meredith for discussions. This research was supported by Natural Environment Research Council grants NE/G004811/1 awarded to J.P. and NE/G004137/1 awarded to M.J.L and G.E.A.S.

Author Contributions

JP, MJL and GEAS conceived the project. AS and GEAS performed the $\delta^{18}O_{diatom}$ analyses. JP performed the wavelet analysis and wrote the manuscript. All authors contributed to interpretations and commented on the manuscript.

Additional Information

The authors declare no competing financial interests. Supplementary information accompanies this paper on www.nature.com/naturegeoscience. Reprints and permissions information is available online at www.nature.com/reprints. Correspondence and requests for materials should be addressed to J.P.

Figure Captions

Figure 1 **Proxy records illustrating potential west Antarctic Peninsula ocean and climate forcing mechanisms** Holocene proxy records from ODP Site 1098, Palmer Deep, plus proxy records from other sites that demostrate ocean and climate forcing meachnisms. **a**, $\delta^{18}O_{diatom}$ from Site 1098 (bar shows analytical reproducibility of 0.3‰ (1 standard deviation)); **b**, relative abundance of the cryophilic marine diatom *Fragilariopsis cylindrus*, ODP Site 1098[4]; **c**, % sand, El Junco Crater Lake, Galápogos[20]; **d**, cholestrol abundance, ODP Site 1228, Peru margin[5]; **e**, dinosterol abundance, ODP Site 1228, Peru margin[5]; **f**, summer (December) insolation at 60ºS[24]; clay/silt ratio, Skyring 1, Southern Chile[15]. Vertical shaded box indicates transition seen in (a) that represents the shift from non-cyclic forcing to cyclic internal forcing of Antarctic climate[14].

Figure 2 **Morlet wavelet analysis of ODP Site 1098 $\delta^{18}O_{diatom}$ record** Lower panel shows the wavelet power spectrum. Shaded contours represent normalised variances and

black lines surround statistically significant regions that exceed 95% confidence for a red noise process. Power in hatched regions (cone of influence) is treated with caution due to the wavelet approaching the end of the finite time series.

Figure 1

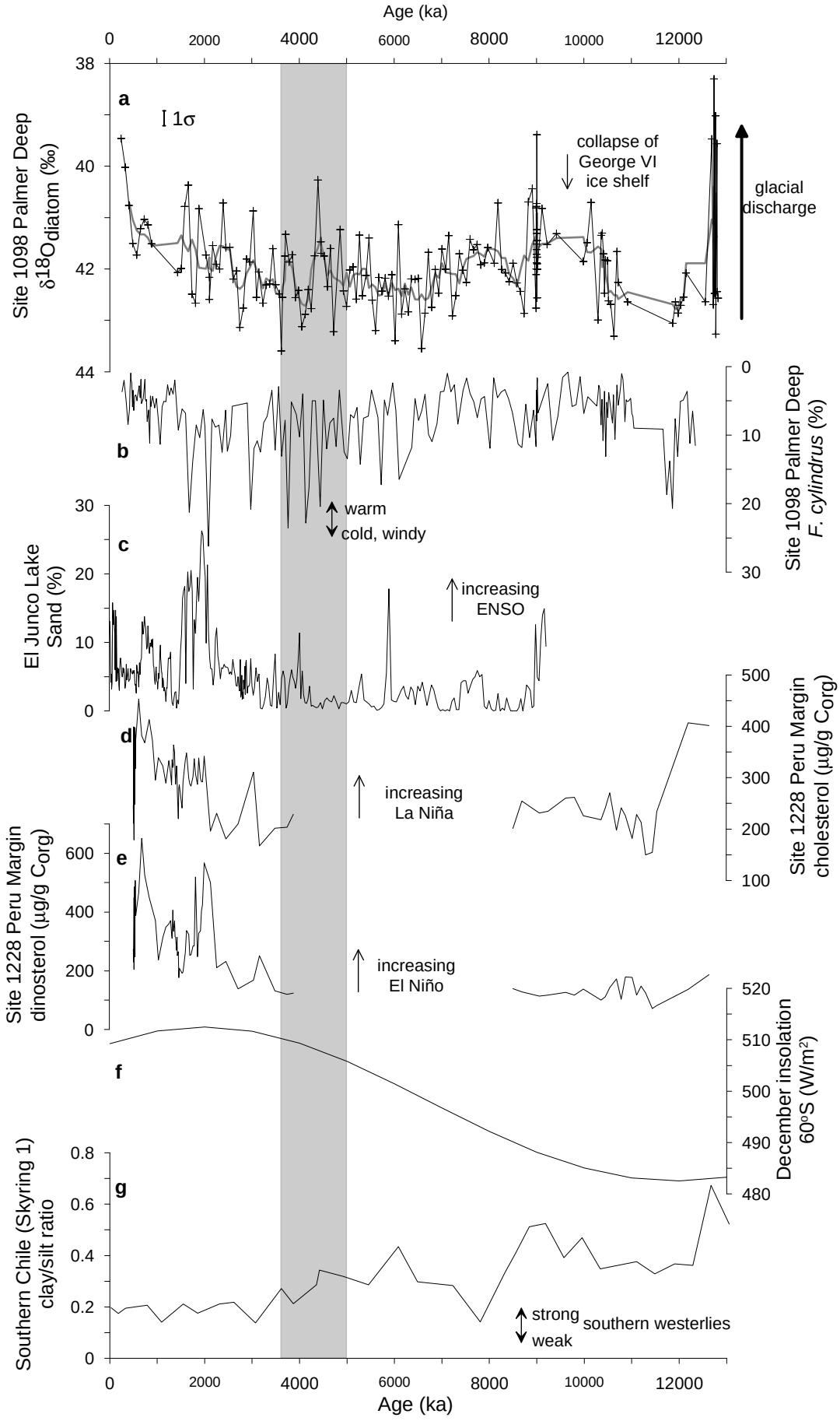
Age (ka)
0
2000
4000
6000
8000
10000
12000
a
1σ
collapse of George VI ice shelf
glacial discharge
Site 1098 Palmer Deep δ18Odiatom (‰)
38
40
42
44
b
warm
cold, windy
Site 1098 Palmer Deep F. cylindrus (%)
0
10
20
30
c
increasing ENSO
El Junco Lake Sand (%)
d
increasing La Niña
Site 1228 Peru Margin cholesterol (µg/g Corg)
100
200
300
400
500
e
increasing El Niño
Site 1228 Peru Margin dinosterol (µg/g Corg)
f
December insolation 60°S (W/m2)
480
490
500
510
520
g
strong
weak
southern westerlies
Southern Chile (Skyring 1) clay/silt ratio
0
0.2
0.4
0.6
0.8
Age (ka)

Figure 2

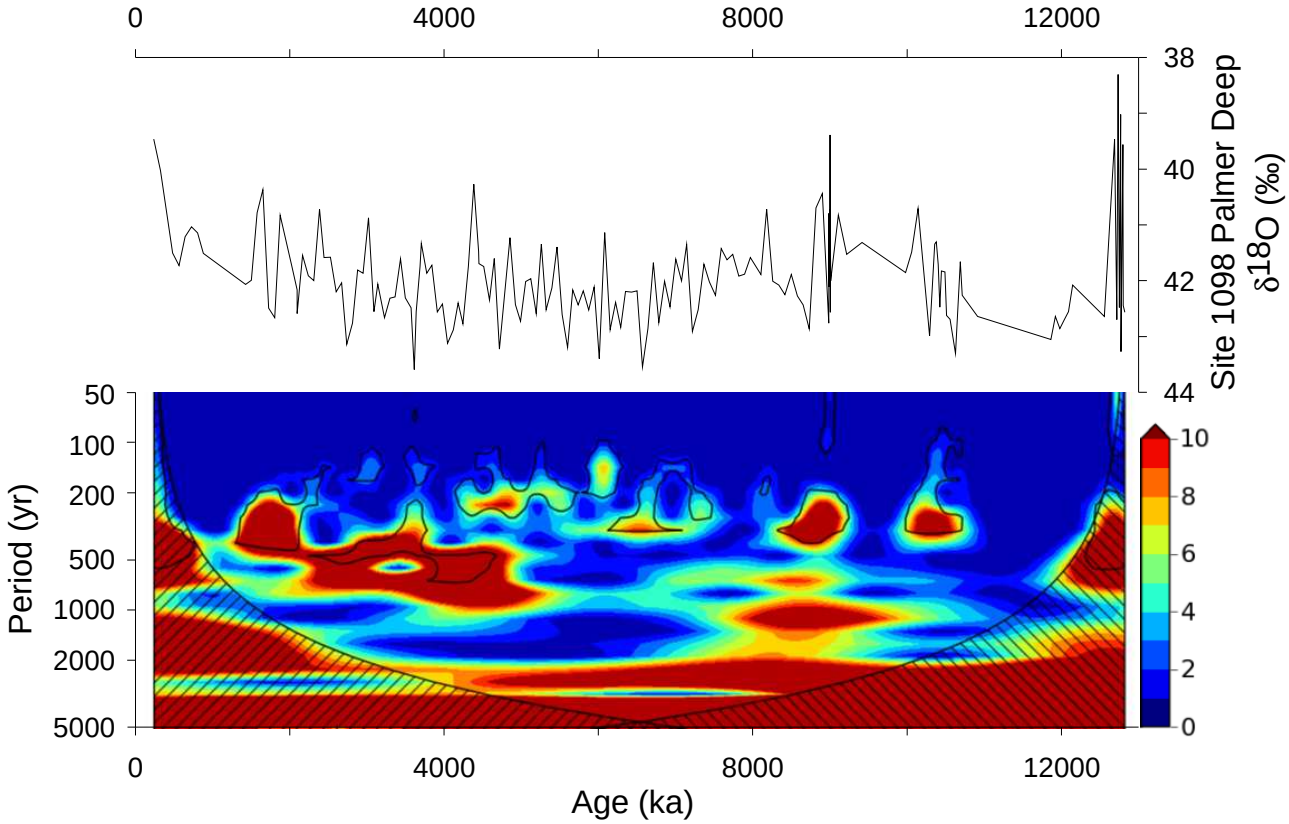
0
4000
8000
12000
38
40
42
44
Site 1098 Palmer Deep
δ18O (‰)
50
100
200
500
1000
2000
5000
Period (yr)
10
8
6
4
2
0
Age (ka)